Geophysical Research Letters

Supporting Information for

The role of atmospheric electric field in the dust lifting process

F. Esposito[1], R. Molinaro[1], C. I. Popa[1], C. Molfese[1], F. Cozzolino[1], L. Marty[1], K. Taj-Eddine[2], G. Di Achille[3], G. Franzese[1,4], S. Silvestro[1], G. G. Ori[5,2]

[1] INAF – Osservatorio Astronomico di Capodimonte, Salita Moiariello 16, 80131 Napoli, Italy
[2] Ibn Battuta Centre - University Cadi Ayyad, 40000, Marrakech, Morocco
[3] INAF-Osservatorio Astronomico di Teramo, 64100, Teramo, Italy
[4] University of Naples "Federico II", Corso Umberto I, 40 - 80138 Napoli, Italy
[5] IRSPS Università G. D'Annunzio, Pescara, Italy

Contents of this file

Introduction

This supporting information provides a brief description of the soil composition in the study sites. In addition, we provide details on the friction velocities and threshold friction velocities values computed for the selected dust storm events.

Text S1.

Soil composition

The soil at both measuring sites is the main source for the atmospheric dust. It has a complex composition, reflecting the various processes involved in its production. The main processes involved are detrital comminution, weathering, and evaporitic crystallization. While detrital products simply represent an accumulation of water eroded and windblown material, the evaporitic products relate to a cumulus of processes (e.g. phyllosilicate cation exchange, evapo-transpiration, efflorescence, etc.). These water interactions provide the Mg^{2+}, Ca^{2+} cations in the solution via ion exchange capacity mainly acting of phyllosilicates (i.e. muscovite, illites, and chlorites). The sediment composition was resolved by using a combination of techniques (XRD, IR spectroscopy, and SEM-EDS) and reflects the erosion of the marine late Paleozoic sediments that constitute the regional bedrock. They are represented by detrital shale grains + quartz + carbonates in the sand fraction. The silt and clay (< 63 μm) fractions share the same composition of the sand fraction, whilst having more free clays/micas released from the comminution of shales. The latter process releases the original detrital particles in the bedrock sedimentary rocks (quartz, muscovite, and chlorites) and the clay minerals in their interstices (represented by the smectite-illite and serpentine-chlorite series). On the other hand, the clay fraction (< 2 μm), is represented by Fe oxides and carbonates, whilst it is depleted in clay minerals (situation probably related to wind deflation).

The evaporite phases are those obtained by quantitative soil leaching a series of filters in cascade (i.e. Whatman 2 μm, and Millipore 0.2 μm), and subsequent oven evaporation at 110°C

of the filtrate. The result is a solid mixture with a composition of major components identified via the SEM-EDS analysis of homogenized pellets. The sites analyzed in 2013 and 2104 campaigns have similar compositions but different amounts of soluble minerals (22% and 3% respectively, after normalizing for water assuming the stable hydration form at the measured conditions). These data reflect the different position with respect to the water table, with the 2013 site being located towards the basin center, while the 2014 right on the basin edge (Table S1). SEM-EDS analyses on individual detrital grains point to the presence of NaSO4·nH2O phases (thenardite-mirabilite series) as grain surface films and crystals (Table S2).

Sample	Water soluble	>63 µm		< 63 µm		Total
	% evaporite	% silicate	% carbonate	% silicate	% carbonate	
2013 crust	22.35	28.76	8.40	27.19	13.30	100.00
2014	3.05	51.52	15.53	19.47	10.44	100.01

Table S1. *The analysis of the soil samples divided for grain size classes for the 2013 and 2014 soils.*

This composition points to the presence of evaporite species with the order of appearance in the following sequence: halite-mirabilite-bischophite-carnallite-tachyhydrite/antarcticite that either cement or cover the bulk silicate/carbonate detrital minerals or form individual crystals. The mineral composition was derived from the chemical analysis using a normative approach as in Bodine and Jones (1986).

O	Na	Mg	Al	Si	S	Cl	K	Ca	Total
17.38778	13.61444	5.212222	0.05	0.056667	0.24	51.52111	0.634444	10.82111	99.53444

Table S2. *Major elements composition of the water-soluble phases computed from the X-ray fluorescence patterns using the K lines for both 2013 and 2014 sites*

The analysis reported shows that the brine from which the minerals derived is of III B1a type (i. e. Na, Ca, Mg, Cl rich) (Eugster, 1980).

Threshold friction velocity

The threshold friction velocity u^*_t is the minimum friction velocity u* required to initiate movement of soil particles. We estimated u^*_t for the events analyzed in this work by using the saltation rate, as measured with Sensit sensors, and the u*, as measured with the 3D anemometer. We computed u^*_t as the u* value at which saltation start to be detected, i.e when the Sensit signal becomes greater than zero. We assumed a power law between Sensit counts and friction velocity (Kok and Renno, 2008):

$$S_{counts} = A(u^*)^B \qquad (1)$$

which can be reduced to a linear equation by taking the logarithm of both members:

$$log(S_{counts}) = n + mlog(u^*) \qquad (2)$$

where $n = \log(A)$ and $m = B$. This linear trend is shown for all selected events in Figure S**Error! Reference source not found.**, where the Sensit counts are plotted against the wind friction velocity, using a log-log scale. The plotted values of u* and Sensit counts have been respectively averaged and summed using a 30 minutes time window. The results of the linear regression are also shown.

The threshold friction velocity is computed from eq. 2 as:

$$u_t^* = 10^{-n/m} \qquad (3)$$

The values of the estimated u^*_t are given in Table S3. From the listed values we obtain a mean value equal to 0.22 (m/s) and a standard deviation 0.07 (m/s).

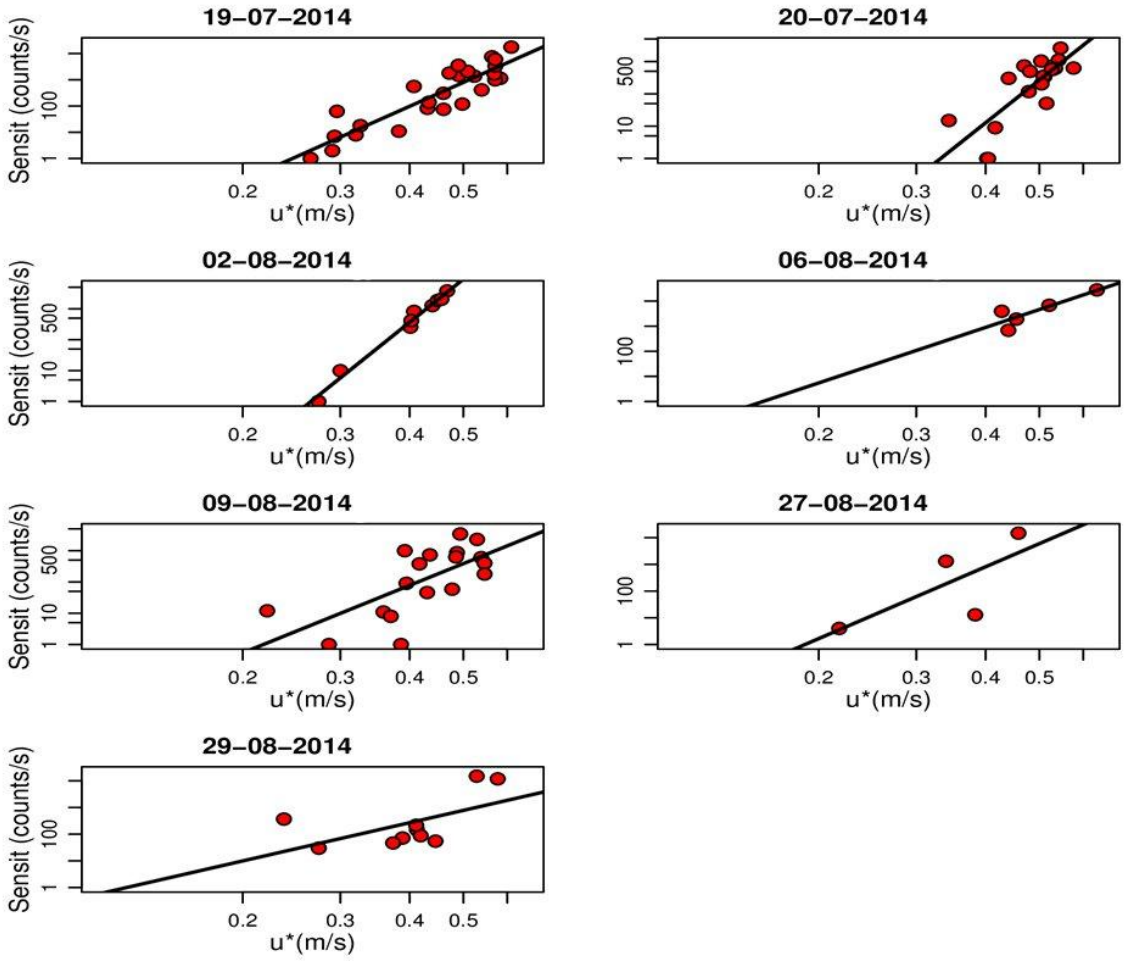

Figure S1: *Log-log scale plot of the Sensit counts against the wind friction velocity estimated through the 3D anemometer. The data of each selected event are represented with red circles, while the solid black line is the result of the linear regression.*

Date	u^*_t
19-07-2014	0.26 ± 0.06
20-07-2014	0.33 ± 0.10
02-08-2014	0.26 ± 0.04
06-08-2014	0.16 ± 0.13
09-08-2014	0.22 ± 0.16
27-08-2014	0.18 ± 0.34
29-08-2014	0.12 ± 0.16

Table S3: *Estimated threshold friction velocity values.*

Computation of the friction velocity

The equation used to compute the friction velocity u* comes from the Monin-Obukhov similarity theory (Kaimal and Finnigan, 1994):

$$u^* = \sqrt[4]{\overline{(u'w')}_o^{\,2} + \overline{(v'w')}_o^{\,2}} \qquad (4)$$

where u, v and w are the wind components along right-handed coordinate axes x, y, and z, respectively. The mean component is denoted by the overbar, while, the prime denotes the eddy. In principle, the momentum flux in the equation (4) should be evaluated at the surface level. In practice, it can be measured at any convenient height z inside the surface layer where its vertical variations can be assumed negligible with height. This condition is reasonable for Kaimal and Finnigan, 1994:

$$\frac{z}{|L|} \lesssim 1 \quad (5)$$

The u* used in this work has been computed from the three components of wind as measured by the 3D anemometer mounted at 4.5 m. We evaluated z/|L| at z = 4.5 m (where the 3D anemometer was mounted) for all the dusty events reported in this work. Figure S2 shows the time evolution of this parameter for each event. The value of z/|L| generally satisfies the stated condition (eq. 5), except for some short time periods where it shows some spikes. Moreover, for the selected events we have also evaluated the friction velocity by the logarithmic wind profile, using 2 different sets of anemometers. The first set is composed of 3 anemometers placed at the height 0.5 m, 1.4 m and 4 m. The second set is composed of 3 anemometers placed at the height 4.5 m, 7 m and 10 m. The comparison of the two u* evaluated at different height shows that their difference Δu* just sporadically exceeds the 50%, and that the mean values of Δu* inside the events are usually compatible with zero within the uncertainties, as

reported in Table S4. All these considerations assure that the u* estimated at 4.5 m from 3D wind measurements represents reasonably the friction wind velocity.

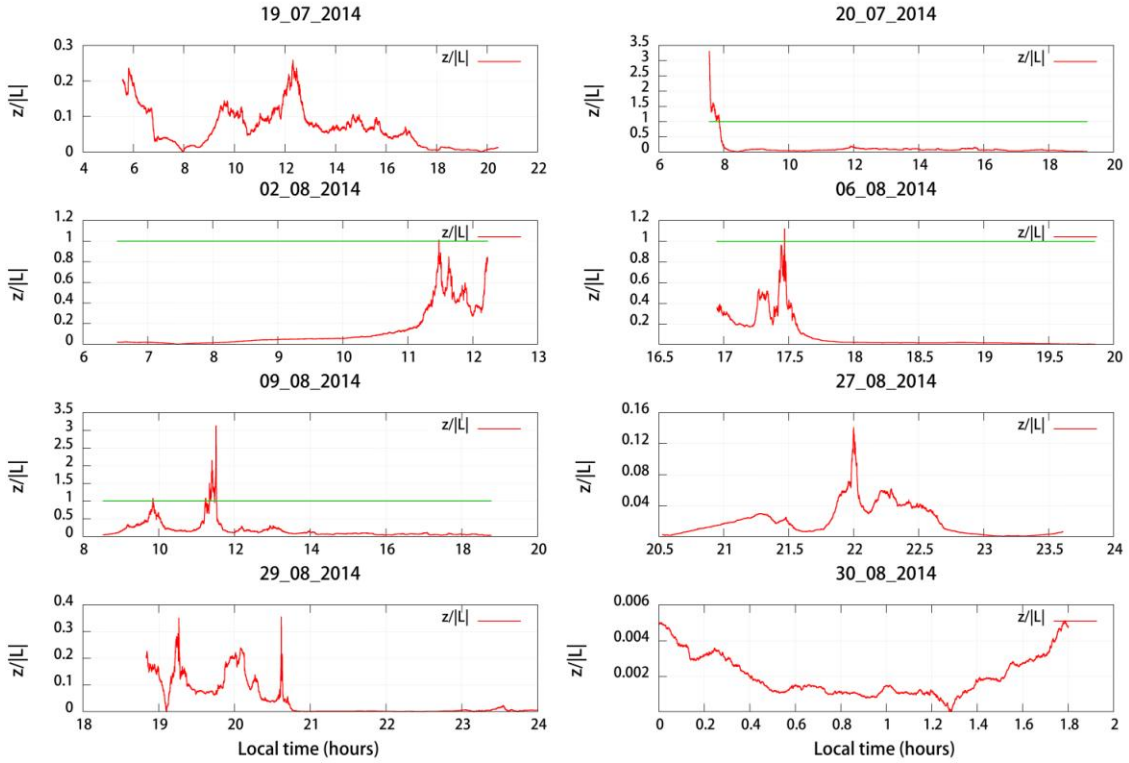

Figure S2: *Time evolution of the stability parameter z/|L| is plotted for each selected event (in red), the threshold f(t)=1 is also plotted (in green).*

Date	Δu*
19-07-2014	0.022 ± 0.12
20-07-2014	-0.054 ± 0.068
02-08-2014	0.062 ± 0.060
06-08-2014	-0.031 ± 0.070
09-08-2014	-0.032 ± 0.071
27-08-2014	0.11 ± 0.054
29-08-2014	0.003 ± 0.13
30-08-2014	0.040 ± 0.061

Table S4: *Difference between the values of the friction threshold evaluated by the second and the first set of anemometers*

References

Bodine Jr, M. W., and B. F. Jones, 1986, The SALT NORM : a quantitative chemical-mineralogical characterization of natural waters, Water-Resources Investigations Report.

Eugster, H. P., 1980, Geochemistry of Evaporitic Lacustrine Deposits: Annual Review of Earth and Planetary Sciences, v. 8, p. 35-63.

Kaimal J C and Finnigan J J 1994 Atmosferic boundary layer flows: Their structure and measurement (New York: Oxford University Press).

Kok J., Renno N. O. (2008b), Electrostatics in Wind-Blown Sand, *Physical Review Letters, vol. 100, Issue 1*, id. 014501.